1986MNRAS.218...75G

Mon. Not. R. astr. Soc. (1986) **218,** 75–91

Planetary surface texture and albedo from parameter plots of optical polarization data

J. E. Geake *Department of Pure and Applied Physics, UMIST, PO Box 88, Manchester M60 1QD*

A. Dollfus *Observatoire de Paris, 92195 Meudon, France*

Accepted 1985 July 22. Received 1985 July 22; in original form 1985 May 8

Summary. Optical reflectance polarization measurements obtained with the Meudon Observatory polarimeter, in the laboratory and on the telescope, are collected together for the first time; surfaces investigated include rock and powder samples, meteorites, lunar samples and atmosphereless planetary bodies. Interpretation of the data involves plotting polarization curve parameters and albedo, two or three at a time; all the types of plot that have been found useful are reviewed, including a new three-dimensional model. The empirical relationships found from these plots, calibrated by using data for known surfaces, are then of use for the remote determination of planetary surface properties, such as surface texture and albedo; a new method of estimating grain size is described.

1 Introduction

The optical polarimeter of the Laboratoire Physique du Systéme Solaire at Paris Observatory, Meudon, is used for laboratory measurements, and also for telescopic measurements of planetary bodies at Meudon and at the Pic-du-Midi Observatory. During 25 years of operation it has produced a large amount of data, which has hitherto been divided between many separate publications. It is now useful to collect the more important data together in one place, for reference purposes, and to review and extend the graphical methods of data analysis.

The main use of the polarization data obtained for planetary surfaces is for the remote discernment of surface texture and optical properties. This method was first used by Lyot (1) in 1929, and its more recent use involving the *Apollo* and *Luna* lunar samples has been summarized by Dollfus & Geake (2).

The principle of the method is based on the observation that when unpolarized light is scattered by a rough surface it becomes partially linearly polarized, and the plane of polarization is usually found to be either normal to the plane containing the incident and observation rays (regarded as positive polarization) or parallel to this plane (regarded as negative). If the scattered light has intensities $I_\perp$ and $I_\parallel$ polarized in directions normal and parallel to the plane of the incident and emergent rays, then the proportional polarization is defined as $P=(I_\perp-I_\parallel)/(I_\perp+I_\parallel)$, usually

Downloaded from https://academic.oup.com/mnras/article/218/1/75/978183 by guest on 20 August 2022

© Royal Astronomical Society • Provided by the NASA Astrophysics Data System

1986MNRAS.218...75G

expressed as a percentage, or in parts per thousand. P is found to change with the phase angle V between the incident and observation rays, and a plot of P against V is found to give a curve characteristic of the surface. Fig. 1 shows a typical curve for a rough granular surface, and defines the parameters found to be diagnostic of surface texture and optical properties. For example, the negative part of the curve may be used to discern surface texture, the slope may be used to estimate the albedo, and the positive peak together with the albedo gives an indication of grain size.

The method of using reflectance polarization measurements has been as follows: first, polarization curves were obtained in the laboratory for a large number of known samples, of a wide range of surface types; then, from these curves, values of the polarization parameters, as shown in Fig. 1, where obtained from each sample. Plotting these parameters and the albedo together, usually in pairs, revealed certain relationships between the parameter values and the albedo and surface texture. These diagrams, thus calibrated, can now be used to discern the properties of unknown surfaces for which some of the polarization parameters have been measured. We have now extended the method to three-parameter plots, in both two and three dimensions.

2 The Meudon polarimeter and goniometer

The photoelectric polarimeter used for the measurements described in this paper was designed and constructed at Meudon Observatory. It is used in null mode, with a thin fused-silica plate as a Fresnel compensator: this is placed between the sample and the polarimeter, and is so tilted and orientated as to introduce polarization opposing that in the beam, thus reducing the polarization of the light reaching the polarimeter. Any remaining polarized component of the light is then modulated, and detected as an alternating signal by a photomultiplier. To make a measurement, the compensating plate is tilted to such an angle that the output signal is zero, and the polarization of the light scattered by the sample is then a known function of this angle. There are two alternative modulators, for use in the laboratory and on a telescope respectively.

The laboratory version has never been described in detail, but there is some information in references 3, 4, 5 and 6. It uses a pressure-activated modulator, because this does not introduce any instrumental polarization: pressure is applied to one end of a fused-silica block by a cam-

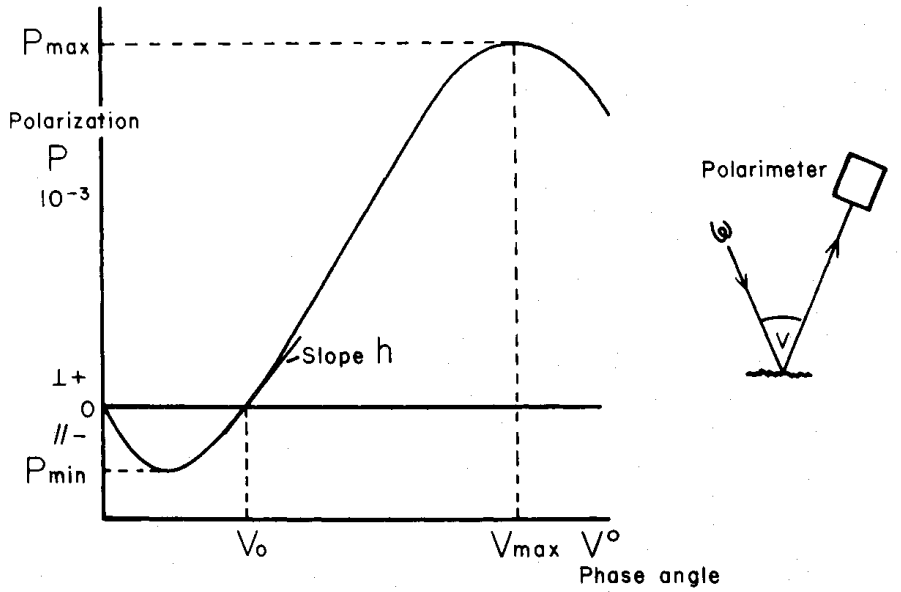

Figure 1. Typical polarization curve for a rough surface, showing how polarization P varies with phase angle V, and defining the parameters used to describe the curve.

Downloaded from https://academic.oup.com/mnras/article/218/1/75/978183 by guest on 20 August 2022

© Royal Astronomical Society • Provided by the NASA Astrophysics Data System

1986MNRAS.218...75G

operated lever, and the stress causes birefringence. The pressure amplitude is adjusted to give half-wave birefringence, which rotates the plane of polarization by 90°.

The alternative modulator for use on a telescope, where mechanical vibration is unacceptable, is based on a rotating sector disc with alternate half-wave plates and gaps (7,8).

For laboratory use, the polarimeter is mounted on one arm of a large vertical goniometer; the other arm carries a tungsten lamp as the light source, and a depolarizing plate. It is able to illuminate a 1 cm-diameter horizontal sample with depolarized light, over a range of phase angles from 2.5° to 160°. The prototype of the polarimeter and the goniometer is described by Marin (5), and a photograph is shown in reference (6).

3 Polarization and albedo data

3.1 PARAMETERS

We shall now list measurements of the polarization curve parameters defined in Fig. 1, and also albedo values, for a range of different types of laboratory sample and for some atmosphereless planetary surfaces. Apart from some samples of special interest, we have only listed laboratory samples for which at least four of the following five parameters have been measured:

P_{min}, the depth of the negative branch,
V_0, the width of the negative branch,
P_{max}, the height of the positive peak,
h, the slope averaged over 10° beyond V_0,
A, the albedo.

The albedo values given were measured by comparison with a smoked MgO screen, with the illumination at normal incidence. A phase angle of 5° was used, as this value was found to give the most reproducible results: at large phase angles surface roughness has a major effect on albedo, and the type of roughness typical of a planetary regolith will not be reproduced in the laboratory; at phase angles near to zero the 'opposition spike' effect, due to deep small-scale cavities, becomes important, and this is also difficult to reproduce in laboratory samples. All our planetary surface albedo measurements were therefore made at, or corrected to, a phase angle of 5° (see references 4, 9, 10).

The laboratory polarization measurements listed were usually made with the incident and emergent rays roughly symmetrical about the normal to the sample plane, i.e. with the normal bisecting the phase angle. It is only with crystalline surfaces of high albedo that departure from this symmetrical position has a significant effect on the polarization produced; this has been investigated in detail by Dollfus (11).

3.2 SURFACE TYPES

The tabulated parameter values collected in this paper are for surfaces of the following types:

Laboratory measurements:
Table 1: Lunar fines.
Table 2: Lunar rocks and breccia freshly broken, with no adhering dust.
Table 3: Lunar rocks and breccia: outer surface, with adhering dust.
Table 4: Meteorite powder.
Table 5: Terrestrial rocks, natural or freshly chipped.
Table 6: Terrestrial rock powder: grain size <50 μm.
Table 7: Terrestrial rock powder: grain size 50–340 μm.

Telescopic measurements:
Table 8: Planets and satellites.

Downloaded from https://academic.oup.com/mnras/article/218/1/75/978183 by guest on 20 August 2022

© Royal Astronomical Society • Provided by the NASA Astrophysics Data System

1986MNRAS.218...75G

Other laboratory samples, for which fewer parameters had been measured, are not listed here, but data may be found in the references given: e.g. for metallic powders in reference 12. Volcanic ashes of a wide range of types were also measured (1, 4); these are not reported here because they tended each to contain a wide range of grain sizes and surface textures, and were thus too heterogeneous for useful deductions to be made for our present purpose.

3.3 ACCURACY

The accuracy of the measurements listed varies over a wide range, depending on such factors as the homogeneity of the samples and the amount of specular reflection from grain facets. Under the best conditions, the highest accuracies achieved for the laboratory measurements are estimated to be as follows:

Polarization $P_{min} \pm 0.5 \times 10^{-3}$ $P_{max} \pm 10 \times 10^{-3}$,
albedo ± 0.01,
slope $\pm 0.05 \times 10^{-3}$ per degree.

In the event, these accuracies are adequately represented by giving all the data to 2½ significant figures, i.e. with the least significant figure either 0 or 5.

Table 1. Lunar fines. From references 2, 10, 13, 14, 15, 16 and Meudon Observatory log book. Sample description: references 9, 13, 17 and NASA documentation.

Sample number	Pmin -10^{-3}	V_0	A	Pmax 10^{-3}	h $10^{-3}/°$
L16.3.7	10.5	22.0	.075	125	1.90
10084.6	11.0	22.0	.075	135	1.70
L16.19.1.116	10.0	22.5	.075	170	1.80
L16.9.7	10.5	22.5	.085	100	1.50
15081.59	9.0	23.0	.090	90	1.25
15601.115	8.5	22.5	.095	95	1.35
15021.158	10.0	23.0	.095	85	1.40
12070.113	10.0	21.5	.100	105	1.60
14003.12	12.5	22.0	.115	90	1.30
15471.67	9.5	22.5	.115	70	1.10
15261.90	10.5	24.0	.120	65	1.15
15271.114	10.0	24.0	.125	60	1.10
15101.130	9.0	24.0	.130	55	1.05
15251.70	10.0	24.5	.130	55	1.15
14163.29	12.0	22.0	.130	75	1.35
15291.55	12.0	23.5	.145	50	0.95
12032.39	9.5	21.5	.150	65	0.95
12033.66	11.0	21.0	.175	55	0.90
L20.19.222	7.5	24.0	.220	25	0.55
67461.19	7.5	23.0	.300	25	0.50
67955.3	3.0	21.0	.595		0.25

Downloaded from https://academic.oup.com/mnras/article/218/1/75/978183 by guest on 20 August 2022

© Royal Astronomical Society • Provided by the NASA Astrophysics Data System

1986MNRAS.218...75G

Table 2. Lunar rocks and breccia, dust-free. From references 9, 10, 13, 15, 18 and Meudon Observatory log book. Sample description: references 9, 10, 13, 15, 18 and NASA documentation.

Sample number	Pmin -10^{-3}	V_0	A	Pmax 10^{-3}	h $10^{-3}/°$
15015.15.24(e)	7.0	13.5	.070	350	2.25
15015.15.24(b)	7.0	15.5	.080	400	1.40
60016.48.6	6.0	9.0	.090		2.00
15015.15.24(2)	8.5	16.5	.090		
10020.42	6.0	12.0	.100	535	1.65
12063.39	3.5	8.5	.135		1.05
12002.102	3.0	10.0	.135	375	
60016.22.6	7.0	16.5	.210	270	0.70
60015.37(1)	15.5	18.5			2.40
60015.37(2)	10.0	15.5			2.05
12051.51	4.0	16.0	.260	320	0.75
14267.(3)	4.0	16.0	.280		0.80
68416.24	1.5	8.0	.300		0.35

3.4 WAVELENGTH

Our measurements are usually made through one of five filters, covering the wavelength range from 3500 to 5800 Å; occasionally others at 3380 or 6200 Å are used. However, all the measurements listed here were made through a filter centred at 5800 Å, with a half-width of about 500 Å.

Table 3. Lunar rocks and breccia, dusty. From references 9, 10, 13, 15, 18 and Meudon Observatory log book. Sample description: references 9, 10, 13, 15, 18 and NASA documentation.

Sample number	Pmin -10^{-3}	V_0	A	Pmax 10^{-3}	h $10^{-3}/°$
15015.15.24(d)	10.5	19.0	.085		
10057.54	9.0	19.0	.085	340	1.90
79035.13 chip	14.0	22.0	.090	130	2.20
10059.36	11.5	21.0	.095	380	1.95
61016.23	9.5	21.0	.095	245	1.40
60015.37	14.5	18.5	.115		2.20
14267.(2)	12.0	19.0	.120		3.00
14267.(4)	11.0	20.5	.120		1.00
14267.(A.12)	10.0	19.0	.120	360	1.30
60015.37(1)	16.0	21.5	.125		2.30
12063.39(1)	10.0	21.0	.155		1.95
12063.39(2,3)	8.0	21.0	.165		1.20
14321.151	7.0	19.5	.185	130	0.80
14083.5	4.0	20.0	.525	145	0.35
67455.3	3.0	20.5	.595	160	0.25

Downloaded from https://academic.oup.com/mnras/article/218/1/75/978183 by guest on 20 August 2022

© Royal Astronomical Society • Provided by the NASA Astrophysics Data System

1986MNRAS.218...75G

Table 4. Meteorite powder. From references 4, 16 and Meudon Observatory log book. Sample description: reference 4; grain sizes: 20 to 340 μm.

Name	class	Pmin -10^{-3}	V_0	A	Pmax 10^{-3}	h $10^{-3}/°$
Achondrites						
Juvinas	EUC	5.0	22.0	.230	50	0.60
Bustee	AUB	4.0	17.0	.280	75	
Kapoeta	HOW	4.5	22.0	.280	55	0.50
Khor Temiki	AUB	4.5	18.5	.320	55	
Bishopville	AUB	2.5	22.0	.350	50	0.60
Tataouine	DIO	2.5	25.0	.490	15	0.25
Tektite						
Dallat		2.0	15.0	.350	70	0.50
Carbonaceous chondrites						
Mighei	CM2	20.0	22.5	.050		3.20
Orgueil	C11	20.0	21.5	.055		2.40
Murchison	CM2	18.0	23.0	.060		3.00
Allende	C3V	11.0	25.0	.100	180	1.60
Karoonda	C04	10.0	18.5	.095	140	1.30
Chondrites						
Abee	E4	12.0	18.5	.095		1.50
Ochansk	H4	6.0	19.0	.140	60	0.90
Daniels Kuils	E6	3.5	18.0	.190	145	
Oubari	LL	6.5	22.5	.230	45	0.80
Pultusk	H5	6.0	22.0	.250	40	0.50
Girgenti	L6	3.5	18.0	.290		0.40
Iron						
Sikhote-Alinski		6.0	18.0	.190		1.80

For other meteorite powder measurements see Zellner et al. ref.18

3.5 APPLICATIONS

The main use of polarization data is for the remote discernment of the surface properties, such as the texture and albedo of atmosphereless planetary surfaces. Before it could be used in this way the method had first to be calibrated, which was achieved by plotting parameter values for a large number of known samples; this revealed relationships between parameter values and surface properties, which can now be used to determine the properties of unknown surfaces for which samples are not available, but for which polarization measurements have been made. We shall later review those parameter relationships which have been found useful for discerning specific planetary surface properties.

4 Albedo determination from the polarization slope parameter *h*

The albedo A of a surface may be estimated by using an empirical relationship between A and h (the slope of the polarization curve as defined in Fig. 1). This relationship was first noted in 1967

Downloaded from https://academic.oup.com/mnras/article/218/1/75/978183 by guest on 20 August 2022

© Royal Astronomical Society • Provided by the NASA Astrophysics Data System

1986MNRAS.218...75G

Table 5. Terrestrial rocks and meteorites, dust-free. From references 1, 4 and Meudon Observatory log book. Sample description: references 1, 4, 17, 19.

Rock type/source	Pmin -10^{-3}	V_0	A	Pmax 10^{-3}	h $10^{-3}/°$
obsidian dark	8.0	5.5	.020	890	2.90
anthrasite	6.0	9.5	.040	980	1.65
lava/Lyot G	4.5	10.0	.045	480	0.95
lava/Lyot F	10.0	15.0	.055	400	1.90
Orgueil meteorite	12.0	15.0	.065		
carborundum	8.5	14.0	.070		
basalt glass/COF	15.0	18.5	.075	530	2.20
andesite/J6,C4	7.0	12.0	.075	540	1.90
ilmenite	13.5	14.0	.080		2.80
lava/Lyot E	5.5	12.5	.085	580	1.90
Allende meteorite	12.0	24.0	.100	320	1.60
porphyr/Lyot B	9.0	15.0	.100	420	2.00
porphyr/Lyot A	6.0	17.0	.120	310	1.60
granite/Lyot B	4.0	13.0	.140	170	0.80
granite grey/Lyot	5.0	16.0	.140	170	0.80
sandstone red/Lyot	10.0	16.5	.145	320	2.00
lava/Lyot C	8.0	17.5	.150	130	
lava/Lyot D	7.0	14.0	.150	220	1.20
lava/Lyot B	5.0	13.0	.150	225	1.00
clay/Lyot	8.0	15.0	.170	160	1.00
labradorite	3.5	15.0	.200		
lava/Lyot A	4.5	12.0	.230	270	1.00
Pultusk meteorite	4.0	16.0	.240	240	0.40
clay white/Lyot	8.0	10.5	.600	210	0.45

by Widorn (27); in 1973 it was further investigated by Ververka & Noland (28) and was calibrated on the basis of lunar sample measurements by Bowell *et al.* (14), who were the first to use it to estimate the albedos of asteroids.

The relationship was refined by Dollfus & Geake (2) using further samples, and in 1977 it was calibrated more precisely by Zellner *et al.* (16, 29) using a wide range of samples including lunar fines and meteoritic and terrestrial rock powders as listed in Tables 1, 4, 6 and 7. Fig. 2 combines the data from references 16 and 19 for all these fines and powdered samples; the relationship is found to be almost independent of grain size and texture, and almost linear (on a log–log scale), except for very dark surfaces with albedos of less than about 5%. The slope h is thus seen to be a useful indication of albedo, as it applies to a wide range of surfaces, and the surface type need not even be known.

This method has now been used to estimate the albedo for 28 asteroids (16, 30, 31, 32), which is useful for type classification. Also, from the albedo and the observed intensity, the average

Downloaded from https://academic.oup.com/mnras/article/218/1/75/978183 by guest on 20 August 2022

© Royal Astronomical Society • Provided by the NASA Astrophysics Data System

1986MNRAS.218...75G

Table 6. Terrestrial rock powder: grain size <50 μm. From references 2, 4, 16, 17, 20 and Meudon Observatory log book. Sample description: references 4, 16, 17, 19.

Rock type/source	Pmin -10^{-3}	V_0	A	Pmax 10^{-3}	h $10^{3}/^{\circ}$	Grain size μm
anthrasite	8.0	12.5	.035		2.75	<50
ilmenite	9.5	16.5	.055		1.80	<50
augite	6.5	18.0	.160	85	0.90	<50
andesite/JG C4	7.5	18.5	.170	70	0.70	<50
basalt BCR	10.0	22.0	.185	55	1.00	
basalt/GF H10	7.5	21.0	.185	40	0.65	<50
hornblende	5.0	17.0	.205	60	0.85	<50
hypersthene	5.5	16.0	.230		0.80	<50
obsidian black	3.0	17.0	.240	45	0.60	<50
peridotite	4.5	19.0	.240	40	0.65	<50
breccia/Meteor Crater	4.0	19.0	.320	30		
olivine	2.0	(15)	.330	30	0.35	<50
glass	1.0	14.0	.430	25	0.30	

Sources: GF = G.Fielder; H = Hawaii
JG = J.Guest; C = Chile
COF = D.Coffeen; SP = Sunset Peak, Arizona
GDN = G.D.Nichols; I = Iceland
AD = A.Dollfus

diameter of the asteroid can be obtained (14), even though it is far too small to be resolved with a telescope.

The qualitative physical explanation of this relationship is probably that the overall scale of the polarization curve is controlled by the degree of dilution by unpolarized diffuse light, and it is this diffuse light that mainly controls to the albedo; thus the higher the albedo, the lower is P_{max}, and consequently the lower the slope of the curve as it rises towards P_{max}.

5 Grain-size determination from P_{max}

As early as 1905 Umov (33) discovered from simple experiments that the polarization maximum P_{max} for light scattered by a solid surface was greatest for dark surfaces and least for highly reflecting surfaces. In due course it became clear that, for fine-grained surfaces, P_{max} is roughly inversely proportional to the albedo. In 1971 Dollfus *et al.* (3, 4, 20) made accurate polarization measurements for small regions on the lunar surface, and also laboratory measurements of powdered terrestrial rock samples, all of which confirmed this reciprocal relationship; it was, however, evident that the size of the grains had a significant effect.

When samples from the lunar surface became available, the relationship was found to apply very accurately to these samples, which had a rather uniform physical structure (Dollfus *et al.* (10); Bowell *et al.* (13)). The matter was reviewed by Dollfus & Geake (2), and we have taken from that paper the reciprocal relationship between A and P_{max} for lunar fines, which is shown in

Downloaded from https://academic.oup.com/mnras/article/218/1/75/978183 by guest on 20 August 2022

© Royal Astronomical Society • Provided by the NASA Astrophysics Data System

1986MNRAS.218...75G

Table 7. Terrestrial rock powder: grain size 50–340 μm. From references 2, 4, 16, 17, 20 and Meudon Observatory log book. Sample description: references 4, 16, 17, 19.

Rock type/source	Pmin -10^{-3}	V_o	A	Pmax 10^{-3}	h $10^{-3}/°$	Grain size μm
basalt glass/COF	12.5	20.0	.050	600	2.50	90-200
basalt glass/COF	13.0	18.0	.050	560	2.50	50-65
augite	12.5	18.0	.055		2.30	200-340
basalt/AD SP			.060	335		200-340
basalt/GF H9 pahoehoe	12.0	20.0	.065	325		<340
basalt/GF H3 aa	9.0	19.0	.070	340	1.60	<340
basalt/GF H1	9.0	18.0	.075	275		<340
hornblende	11.0	17.0	.095		1.80	200-340
basalt/GF H10	9.0	20.0	.095	240	1.50	<340
basalt/GF H8 ankaramite	9.0	20.5	.100	210		<340
basalt/GF H2 + olivine	8.0	18.0	.105	200		<340
ignimbrite/JG I			.110	190		<340
basalt/GF H5			.115	175		<340
basalt/GF H11 trachyte	7.0	18.0	.120	160		
basalt/GF H4 picrite	6.0	16.0	.125	170		<340
basalt/GF H6 glassy	8.0	21.0	.140	150		<340
peridotite	9.5	19.0	.145	135	1.30	200-340
basalt/GF H7 trachyte	6.0	20.0	.250	45	0.80	<340
labradorite	4.0	15.0	.200		0.75	200-340
ignimbrite/JG C207	2.5	17.0	.200	80		<340
obsidian light	1.5	9.0	.410	30		25-200
ignimbrite/JG C90 dacite	2.5	14.0	.430	35	0.50	<340
syenite/GDN 453	2.0	21.5	.490	15		100
ignimbrite/JG C5			.500	20		<340
granite/GDN 1110	2.0	22.0	.560	15		100

Fig. 3 as a straight line (on a log–log scale). The relationship is indeed so accurately followed in the case of lunar fines samples, that telescopic measurement of P_{max} remains the most precise method of determining the albedo of a lunar area; this method does not require any photometric reference source, or any atmospheric transparency correction. The only reference standard required, in order to calibrate the method, is the white surface used to measure the albedo values of lunar samples in the laboratory.

This albedo/P_{max} relationship is therefore well established for lunar fines samples, and as a method of measuring the albedo of the Moon it provides an alternative to the albedo/slope relationship described in the previous section. However, when similar laboratory measurements were made for powdered terrestrial rocks, the results were not in agreement with those for the lunar fines samples. Fig. 3 shows some of the results: the line shown for lunar fines is taken from reference 2 and involves data from Table 1: all the points for terrestrial samples are found to lie

Downloaded from https://academic.oup.com/mnras/article/218/1/75/978183 by guest on 20 August 2022

© Royal Astronomical Society • Provided by the NASA Astrophysics Data System

1986MNRAS.218...75G

Table 8. Planets and satellites.

Name	From ref.	Pmin $\times 10^{-3}$	V_o	A	Pmax 10^{-3}	n $10^{-3/\circ}$	Max Obs. V°
							**
Planets							
Mercury	21	14.5	25.0	.095	72	1.40	180
Mars	22,23	11.0	24.0	.140	67 *	1.10	47
Satellites							
Moon, average	3	12.0	23.0	.100	78	1.40	180
Jupiter	24						
J I Io		2.0	11.0	.680	----	----	11
J II Europa		1.0	9.5	.650	----	0.20	11
J III Ganymede		2.0	9.0	.460	----	0.50	11
J IV Callisto front		9.0	(21)	.140	----	----	11
back		6.0	(13)	.140	----	0.95	11
Saturn							
ring B	25,26	3.0	(8)	.60	----	(0.8)	6

** From Earth

* From Mars 5 spacecraft, orbiting Mars

above this line. Points are shown for two size ranges of rock powders, as separated by sieving: <50 μm from Table 6 (triangles); and 50–340 μm (but probably mostly in the range 200–340 μm) from Table 7 (dots). It is evident that these two sets of points lie around different but roughly parallel straight lines, which are displaced from the line for the lunar fines. Further points are shown for solid rocks, both in their natural state, with some surface dust (open circles), and with all the dust removed (crossed circles); all these points lie above those for the powder samples. These straight lines each represent a relationship of the type: $\log P = a \log A + b$, and least-squares analysis of the data gives values of a and b as follows:

	a	b
lunar fines	−1.50	3.47
terrestrial powders<50 μm	−1.38	3.54
terrestrial powders ~200–340 μm	−1.34	3.65

The lunar fines samples contain the smallest grains of any naturally occurring material that we have investigated, having a dominant grain size that we estimate to be about 10 μm, with a range from less than 1 μm to several tens of μm. We also note an empirical boundary, shown as a dotted line in Fig. 3, below which none of our measurements have ever appeared; for this line $a=-1.50$ and $b=3.36$.

The slope coefficient a does not appear to show any simple relationship, but the displacement coefficient b is found to have a roughly linear relationship with log (grain size), as shown in Fig. 4. We now interpret the 'lower limit' line as representing the smallest grain size we ever observe, and we have estimated this to be between 1 and 2 μm. In spite of the rather crude grain-size data, a roughly linear relationship emerges from Fig. 4, between b and log (grain size); this therefore provides the basis of a method of remotely estimating the dominant grain size for a planetary surface, for which values of A and P_{max} can be measured independently; b can thus be calculated,

Downloaded from https://academic.oup.com/mnras/article/218/1/75/978183 by guest on 20 August 2022

© Royal Astronomical Society • Provided by the NASA Astrophysics Data System

1986MNRAS.218...75G

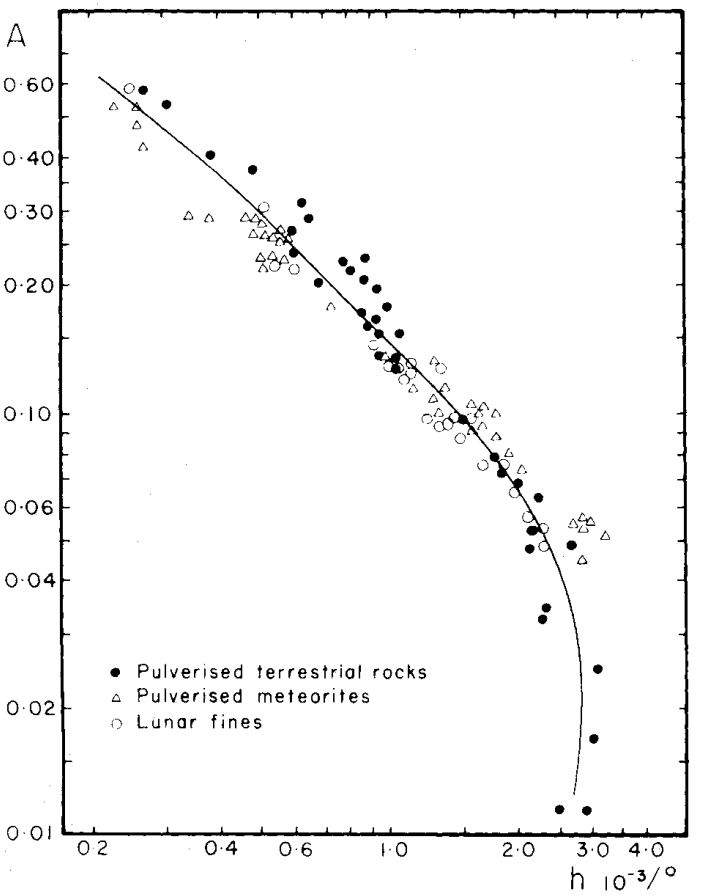

Figure 2. Polarization curve slope h versus albedo A, for pulverized terrestrial rocks (50–340 μm), pulverized meteorites (20–340 μm) and lunar fines. The curve thus established may be used to determine the albedo of an unknown powder surface, from its value of h.

and the empirical relationship shown in Fig. 4 then gives the effective size of the grains which contribute most to the scattered light intensity. It is intended to refine this relationship by laboratory measurements using a wide range of well-defined grain sizes.

With telescopic observation from the Earth, this method can only be used for Mercury and the Moon, as these are the only atmosphereless planetary objects that can be observed at a large enough phase angle to include P_{max} (see Table 8); for all other planetary objects, an orbiting or passing spacecraft is necessary. The method has indeed now been used to estimate the grain size for several different regions of Mars, using data from the USSR–France polarimeter VPM (23) on board the spacecraft *Mars-5,* in orbit around Mars.

6 Surface texture determination from negative polarization

6.1 TWO-PARAMETER PLOT: P_{min} AND V_0

The shape of the negative branch of the polarization curve (Fig. 1) is determined by multiple scattering of light by surface features. Semi-empirical theoretical models have been developed to explain this process, such as those by Öhman (34), Steigmann (35) and Wolff (36, 37, 38); the role of double Fresnel reflection has been demonstrated experimentally by Geake *et al.* (39).

It has been shown by Dollfus & Geake (2, 15) that a plot of the depth of the negative branch

Downloaded from https://academic.oup.com/mnras/article/218/1/75/978183 by guest on 20 August 2022

© Royal Astronomical Society • Provided by the NASA Astrophysics Data System

1986MNRAS.218...75G

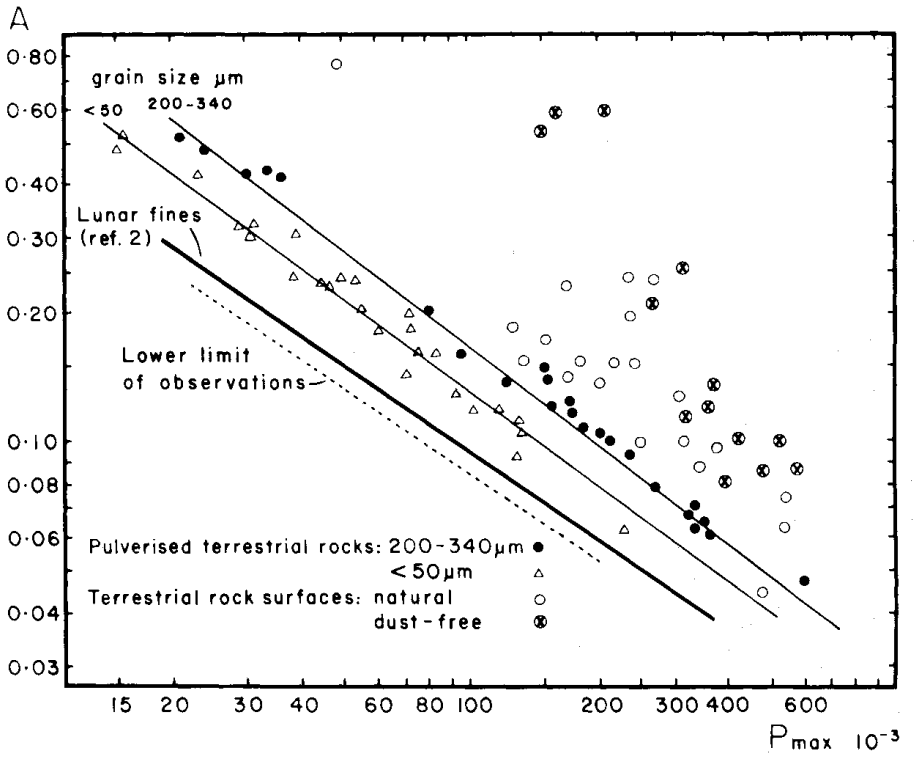

Figure 3. Albedo A versus P_{max}, for lunar and terrestrial samples. Each grain size defines a line represented by the equation: log $P_{max}=a$ log $A+b$, where a=gradient (about 1.4 in each case and b=intercept coefficient, as plotted in Fig. 4.

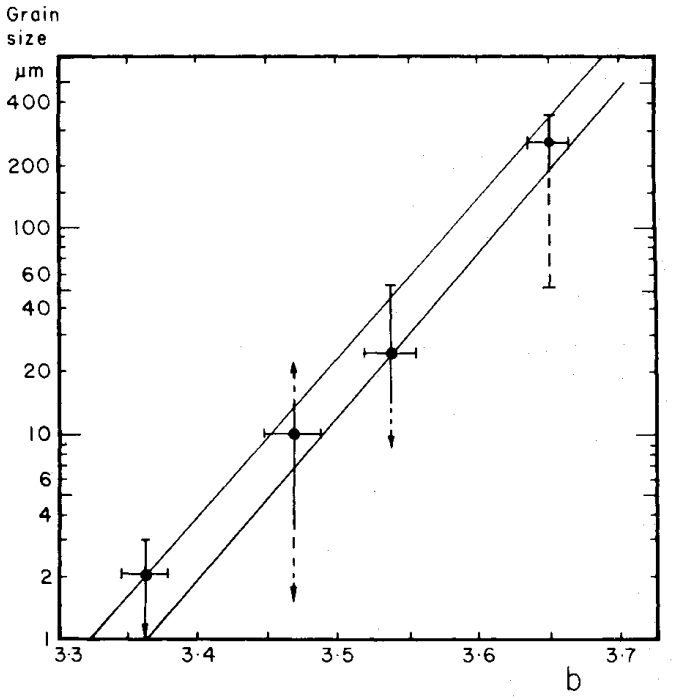

Figure 4. Grain diameter versus intercept coefficient b, as defined in Fig. 3. The rough relationship thus established by the band betwen the lines may be used to estimate the grain size for an unknown surface, from its values of A and P_{max}.

Downloaded from https://academic.oup.com/mnras/article/218/1/75/978183 by guest on 20 August 2022

© Royal Astronomical Society • Provided by the NASA Astrophysics Data System

1986MNRAS.218...75G

(P_{min}) against its width (V_0) may be used to determine surface texture remotely. Fig. 5(a) shows such a plot for laboratory measurements of lunar samples. The sample surfaces were of three main types: fines consisting of dust from the lunar regolith; rock or breccia chips showing the external surface, with some adhering dust particles as revealed by a scanning electron microscope; and the internal faces of freshly broken chips, with no adhering dust. These three types of surface are seen to occupy three separate zones on the diagram. Even this rough division of surfaces into three types is of considerable use in investigating planetary surfaces: Fig. 5(b) shows the three zones copied from Fig. 5(a), superimposed on data for a range of atmosphereless planetary surfaces, as discussed later.

6.2 THREE-PARAMETER PLOT: P_{min}, V_0 AND A

The relationship between polarization parameters and surface properties is shown more clearly on plots involving albedo as a third parameter. This plot may still be in two dimensions, with the third parameter represented by some sort of visual coding of each point; or the plot may actually be constructed in three dimensions, which is much easier to comprehend and to use, but can only be shown in print as a two-dimensional photograph or perspective drawing.

6.2.1 Two-dimensional plot of three parameters

The two-parameter plots of P_{min} and V_0 shown in Fig. 5 may be extended to three parameters by coding each point to represent the albedo value. Fig. 6 shows one way of doing this, with each point drawn as a miniature 'pie diagram'. The plot has here been split into three separate

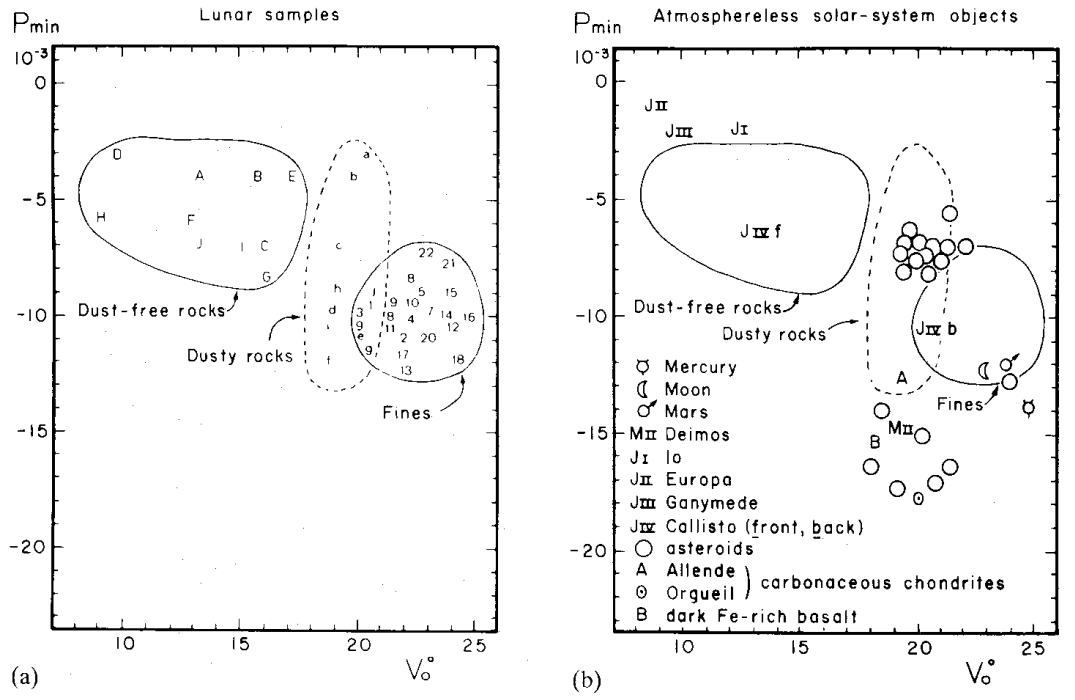

Figure 5. Width V_0 versus depth P_{min} for the negative part of the polarization curve: (a) for lunar samples: fines (numbers), dusty rocks (lower-case letters) and dust-free rocks (capital letters) are seen to occupy three different regions; includes data from Table 1, 2 and 3. (b) For atmosphereless solar system objects; the boundaries of the three regions in (a) are superimposed. (From reference 10.).

Downloaded from https://academic.oup.com/mnras/article/218/1/75/978183 by guest on 20 August 2022

© Royal Astronomical Society • Provided by the NASA Astrophysics Data System

1986MNRAS.218...75G

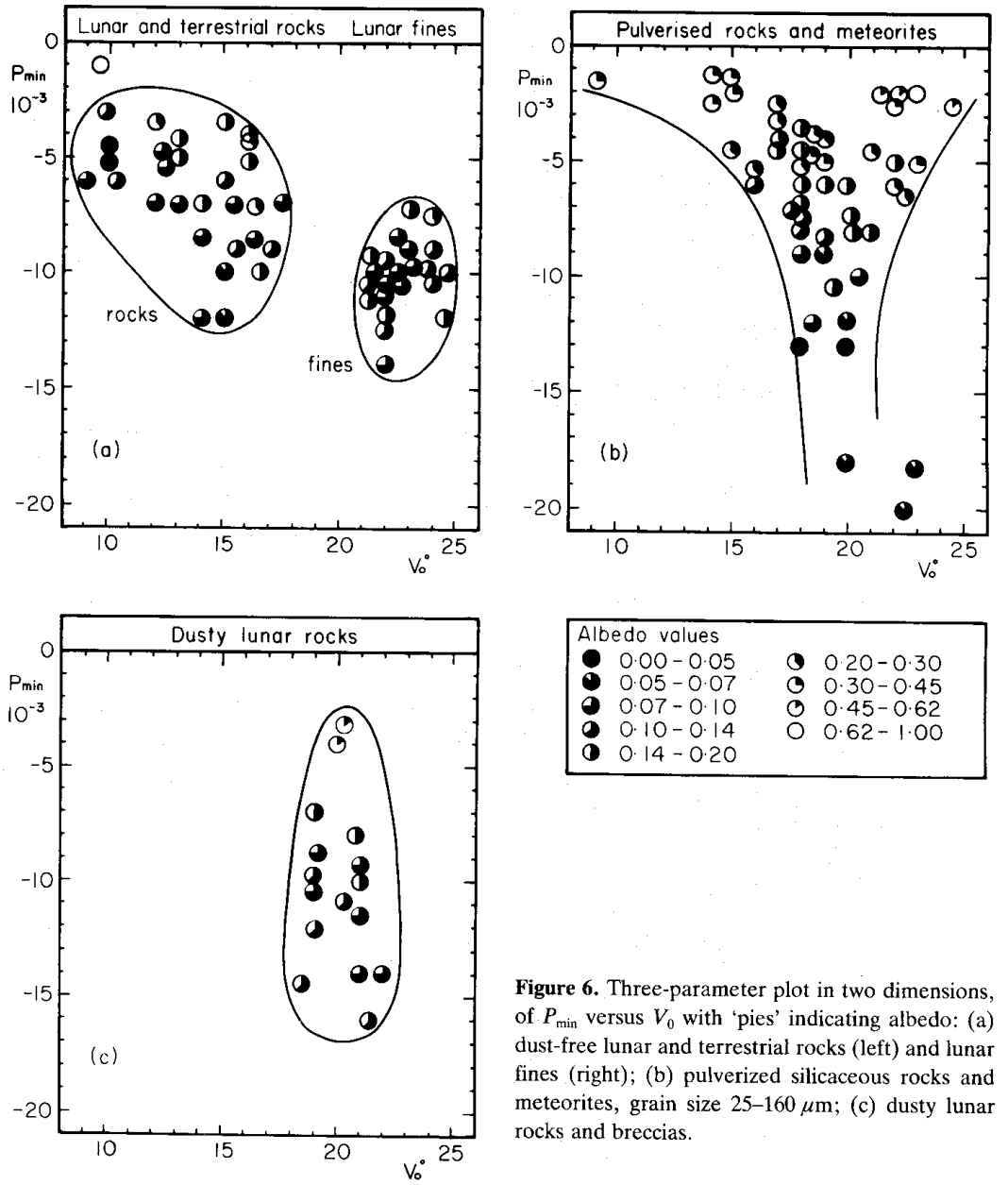

Figure 6. Three-parameter plot in two dimensions, of P_{min} versus V_0 with 'pies' indicating albedo: (a) dust-free lunar and terrestrial rocks (left) and lunar fines (right); (b) pulverized silicaceous rocks and meteorites, grain size 25–160 μm; (c) dusty lunar rocks and breccias.

diagrams covering three groups of samples, for clarity. A similar plot for asteroids has already been published by Dollfus *et al.* (40); all except the M-type asteroids occupy the zone on Fig. 6(b) corresponding to coarse-grained silicacious powders.

As in Fig. 5, the three types of surface represented by the three zones are clearly differentiated; in addition, a general trend can now be seen – that the lower the albedo, the larger the amount of (negative) polarization. This suggests that Umov's law, as discussed in Section 5 for P_{max}, may also apply to P_{min}; however, the form of the relationship is not evident from this two-dimensional three-parameter plot, and to elucidate this a true three-dimensional plot was constructed.

6.2.2 *Three-dimensional plot of three parameters*

The same information may be plotted in three dimensions by plotting P_{min} and V_0 in two dimensions, and then representing each point by a bead on the end of a vertical stem, of length

Downloaded from https://academic.oup.com/mnras/article/218/1/75/978183 by guest on 20 August 2022

© Royal Astronomical Society • Provided by the NASA Astrophysics Data System

1986MNRAS.218...75G

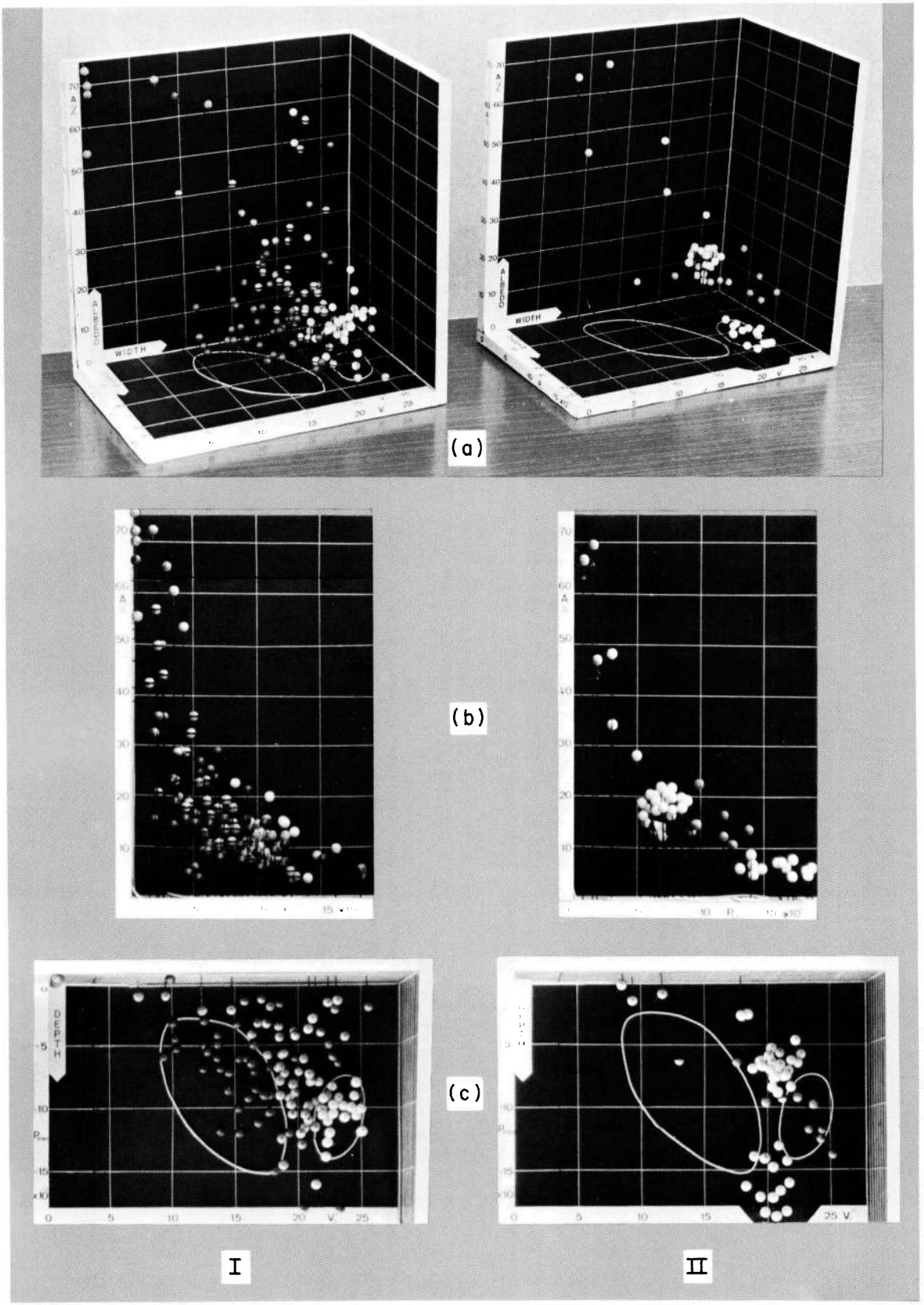

Plate 1. Three-parameter plots in three dimensions, of depth P_{min} versus width V_0 of the negative part of the polarization curve (in the horizontal plane), versus albedo (vertical): I: for terrestrial rocks and powders, and lunar samples; II: for atmosphereless Solar System objects; (a) general view; (b) side view, showing P_{min}/albedo relationship; (c) plan view, equivalent to Fig. 5.

[*facing page* 88]

Downloaded from https://academic.oup.com/mnras/article/218/1/75/978183 by guest on 20 August 2022

© Royal Astronomical Society • Provided by the NASA Astrophysics Data System

1986MNRAS.218...75G

Downloaded from https://academic.oup.com/mnras/article/218/1/75/978183 by guest on 20 August 2022

© Royal Astronomical Society • Provided by the NASA Astrophysics Data System

1986MNRAS.218...75G

proportional to the albedo. Two such models have been made, as shown in Plate 1: one is for laboratory measurements of samples, and the other is for telescopic measurements of atmosphereless planetary bodies. Vertical views of these models as shown in Plate 1(b) are equivalent to Figs 5 and 6, whereas a view from the side as in Plate 1(c) shows the actual form of the P_{min}/albedo relationship, which is indeed reciprocal as in Umov's law for P_{max}. Although not apparent in Plate 1, the beads are also colour-coded to indicate different sample types, and are numbered to identify the individual samples. There is therefore far more information in these models than can be shown with the same clarity in a two-dimensional plot, and being able to view them from any angle has proved to be a useful aid to the thought process of data interpretation. They are shown here purely for illustration purposes: to be of any use, the actual models must be available.

6.2.3 Two-dimensional representation of a three-dimensional plot

An alternative to these three-dimensional models is to use a computer graphics program to generate a perspective view of such as plot. This may be rotated on the screen, and printed out from any chosen viewpoint. It can be explored on the screen with almost the same facility as an actual model, and it has the advantage of making it easier to correct or add data.

6.3 DEDUCTIONS FROM PLOTS

The different types of plot described have now been used to deduce the properties of planetary surfaces, e.g. for Mercury (21), the Moon (2.3), Mars (22, 23), the Galilean satellites of Jupiter (24, 30), C, S and E-type asteroids (31, 40), M-type asteroids (12, 25, 26), and ring B of saturn (25, 26). The three-dimensional models were found particularly useful by Dollfus & Zellner (31), for the interpretation of asteroid surface data. Some of the deductions from all these plots will now be summarized.

6.3.1 A lunar sample in the laboratory is found to match telescopic measurement of its point of origin on the Moon, showing that whatever gives the lunar regolith its characteristic optical properties has not been disturbed by digging up a sample and subsequently exposing it to the Earth's atmosphere.

6.3.2 The point shown in Fig. 5(b) for the Moon is the average for the whole disc; it falls within the zone in Fig 5(a) containing laboratory measurements of lunar fines. Furthermore, all localized measurements of 10-arcsec patches on the Moon's surface (not shown) also fall in this zone, implying that all the places observed on the Moon are regolith-covered, without any significant amount of bare rock.

6.3.3 The point shown in Fig. 5(b) for the whole disc of Mercury falls in the same zone as the lunar fines, although it is near the edge, which suggests that the surface of Mercury also has a regolith of the lunar type, possibly with a larger proportion of the smallest particles.

6.3.4 Mars also has a regolith, as shown by the point for the whole disc in Fig. 5(b). Recent measurements of P_{max} made by the Soviet spacecraft *Mars-5* in orbit round Mars, indicate that the grain size is coarser than for the Moon (Dollfus *et al.* (23)) An average grain size of 20 μm was found for wind-blown dust on the plains, but 40-μm grains were found on some tectonized terrains; even larger sizes were found on a few specific areas, such as the outer edges of large craters.

6.3.5 All the asteroids are different from the lunar regolith, and resemble dusty rock as in Fig. 5(a); more detailed analysis by Dollfus & Zellner (31), shows that they do indeed have a regolith, but that the grain size is larger than for the Moon, Mercury and Mars. The majority of the asteroids have polarization characteristics which divide them into two distinct groups, now

Downloaded from https://academic.oup.com/mnras/article/218/1/75/978183 by guest on 20 August 2022

© Royal Astronomical Society • Provided by the NASA Astrophysics Data System

1986MNRAS.218...75G

identified as S (silicaceous) and C (carbonaceous). The C asteroids resemble carbonaceous chondrite meteorites, and the Martian satellite Deimos (MII in Fig. 5b) is evidently similar. A few of the asteroids, such as 16 Psyche and 21 Lutetia, show distinctively different polarimetric characteristics. They are simulated by pulverized metallic grains, rather than by a silicaceous regolith (Dollfus *et al.* (12)), and they have been classified as type M.

6.3.6 Jupiter's outermost satellite Callisto is shown to have different types of surface on its leading and trailing faces, as phase-locked in its orbit round Jupiter: the leading face resembles the lunar regolith, whereas the trailing face appears to be dust-free rock (24, 41).

6.3.7 Saturn's rings show complex polarization characteristics, which result from the combined effects of directly reflected light, and light multiply scattered between the particles forming the rings. The directly reflected light shows polarization characteristics typical of large particles, at least several millimetres across, which is consistent with the suggestion that they are blocks of dirty ice. In the UV, the polarization is dominated by a haze of much smaller particles; this polarization is due to multiple scattering and is variable with time, indicating some organization of the particles in ephemeral alignments (26, 42, 43).

Acknowledgments

This paper includes data based on laboratory work and measurements at Observatoire de Paris at Meudon, with contributions by E. Bowell, L. M. Dougherty, M. Duseaux, T. Lebertre, J. C. Mandeville, J. P. Perrault, G. A. Steigmann, C. Titulaer and B. H. Zellner. We are grateful to the British Museum (Natural History), to the Museum National d'Histoire Naturelle in Paris, to the National Research Council of Canada, to NASA and to the USSR Academy of Sciences, for the loan of terrestrial, lunar and meteorite samples; also to individuals who lent us samples: P. Authier, A. Cailleux, D. Coffeen, G. Fielder, M. Gaffey, J. E. Guest, G. P. Kuiper, J. Orcel and B. H. Zellner. We are grateful for financial support from CNRS and the Observatoire de Paris, and, at UMIST, from the SERC.

References

1. Lyot, B., 1929. *Annales de L'Observatoire de Paris, Meudon,* **8,** No. 1; or *NASA Technical Translation TT F-187,* Washington DC, 1964.
2. Dollfus, A. & Geake, J. E., 1977. *Phil. Trans. R. Soc. A,* **285,** 397.
3. Dollfus, A. & Bowell, E., 1970. *Astr. Astrophys.,* **10,** 29.
4. Dollfus, A., Bowell, E. & Titulaer, C., 1971. *Astr. Astrophys.,* **10,** 450.
5. Marin, M., 1965. *Rev. d'Opt.,* **44,** 115.
6. Dollfus, A., 1965. *The nature of the lunar surface, Proc. IAU–NASA Symp.,* Johns Hopkins Press, Baltimore, Ch. 8.
7. Dollfus, A., 1963. *Compt. Rend. Acad. Sci.,* **256,** 1920.
8. Dollfus, A., 1974. In: *Planets stars and nebulae studied with polarimetry,* p. 695, ed. Gehrels, T., University of Arizona Press.
9. Geake, J. E., Dollfus, A., Garlick, G. F. J., Lamb, W., Walker, G., Steigmann, G. A. & Titulaer, C., 1970. *Proc. Apollo 11 Lunar Sci. Conf., Geochim. Cosmochim. Acta Suppl. 1,* **3,** 2127.
10. Dollfus, A., Geake, J. E. & Titulaer, C., 1971. *Proc. 2nd Lunar Sci. Conf., Geochim. Cosmochim. Acta Suppl. 2,* **3,** 2285.
11. Dollfus, A., 1956. *Ann. Astrophys.,* **19,** 83.
12. Dollfus, A., Mandeville, J. C. & Duseaux, M., 1979. *Icarus,* **37,** 124.
13. Bowell, E., Dollfus, A. & Geake, J. E., 1972. *Proc. 3rd Lunar Sci. Conf., Geochim. Cosmochim. Acta Suppl. 3,* **3,** 3103.
14. Bowell, E., Dollfus, A., Zellner, B. H. & Geake, J. E., 1973. *Proc. 4th Lunar Sci. Conf., Geochim. Cosmochim. Acta Suppl. 4,* **3,** 3167.
15. Dollfus, A. & Geake, J. E., 1975. *Proc. 6th Lunar Sci. Conf., Geochim. Cosmochim. Acta Suppl. 6,* **3,** 2749.
16. Zellner, B. H., Geake, J. E., Lebertre, T., Duseaux, M. & Dollfus, A., 1977. *Proc. 8th Lunar Sci. Conf., Geochim. Cosmochim. Acta Suppl. 8,* **3,** 1291.

Downloaded from https://academic.oup.com/mnras/article/218/1/75/978183 by guest on 20 August 2022

© Royal Astronomical Society • Provided by the NASA Astrophysics Data System

1986MNRAS.218...75G

17. Hua, C. T., Dollfus, A. & Mandeville, J. C., 1976. *Proc. 7th Lunar Sci. Conf., Geochim. Cosmochim. Acta Suppl. 7,* **3,** 2605.
18. Dollfus, A., 1971. In: *Physical studies of minor planets,* p. 95, ed. Gehrels, T., NASA SP267.
19. Dollfus, A., Crilleux, A., Cerville, B., Hua, C. T. & Mandeville, J. C., 1980. *Geochim. Cosmochim. Acta,* **44,** 1293.
20. Dollfus, A. & Titulaer, C., 1971. *Astr. Astrophys.,* **12,** 199.
21. Dollfus, A. & Auriere, M., 1979. *Icarus,* **23,** 465.
22. Dollfus, A. & Focas, J., 1969. *Astr. Astrophys.,* **2,** 63.
23. Dollfus, A., Deschamps, M. & Ksanfomaliti, L. V., 1983. *Astr. Astrophys.,* **123,** 252.
24. Dollfus, A., 1975. *Icarus,* **23,** 465.
25. Dollfus, A., 1979. *Icarus,* **37,** 404.
26. Dollfus, A., 1979. *Icarus,* **40,** 171.
27. Widorn, T., 1967. *Ann. Univ. Sternw. Wien,* **27,** 112.
28. Ververka, J. & Noland, M., 1973. *Icarus,* **19,** 230.
29. Zellner, B. H., Lebertre, T. & Day, K., 1977. *Proc. 8th Lunar Sci. Conf., Geochim. Cosmochim. Acta Suppl. 8,* **3,** 1111.
30. Zellner, B. H., Gehrels, T. & Gradie, J., 1974. *Astr. J.,* **79,** 1100.
31. Dollfus, A. & Zellner, B. H., 1979. In: *Asteroids,* p. 170, ed. Gehrels, T., University of Arizona Press.
32. Zellner, B. H. & Gradie, J., 1976. *Astr. J.,* **81,** 262.
33. Umov, N., 1905. *Phys. Zevt.,* **6,** 20.
34. Öhman, Y., 1955. *Ann. Stockholm. Obs.,* **18,** 118.
35. Steigmann, G. A., 1978. *Mon. Not. R. astr. Soc.,* **185,** 877.
36. Wolff, M., 1975. *Appl. Opt.,* **14,** 1395.
37. Wolff, M., 1980. *Icarus,* **44,** 780.
38. Wolff, M., 1981. *Appl. Opt.,* **20,** 2493.
39. Geake, J. E., Geake, M. & Zellner, B. H., 1984. *Mon. Not. R. astr. Soc.,* **210,** 89.
40. Dollfus, A., Geake, J. E., Mandeville, J.-C. & Zellner, B. H., 1977. In: *Comets, asteroids and meteorites: interrelations, evolution and origins,* p. 243, University of Toledo Press.
41. Mandeville, J.-C., Geake, J. E. & Dollfus, A., 1980. *Icarus,* **41,** 343.
42. Dollfus, A., 1979. *Icarus,* **39,** 404.
43. Dollfus, A., 1984. In: *Planetary rings,* p. 121, ed. Brahic, A., CNAS.

Downloaded from https://academic.oup.com/mnras/article/218/1/75/978183 by guest on 20 August 2022

© Royal Astronomical Society • Provided by the NASA Astrophysics Data System